Optical Materials: X 22 (2024) 100300

Contents lists available at ScienceDirect

Optical Materials: X

journal homepage: www.journals.elsevier.com/optical-materials-x

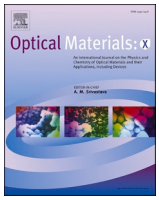

Novel lanthanide-doped $Y_{3-x}Na_xAl_{5-y}V_yO_{12}$ garnets: Synthesis, structural and optical properties

Diana Vistorskaja [a], Arturas Katelnikovas [a], Carlos Martin Signes [b,c], Vytautas Klimavicius [b], Anna Lukowiak [d], Wieslaw Strenk [d], Aivaras Kareiva [a,*]

[a] Department of Inorganic Chemistry, Vilnius University, Naugarduko 24, LT-03225, Vilnius, Lithuania
[b] Institute of Chemical Physics, Vilnius University, Sauletekio 3, LT-10257, Vilnius, Lithuania
[c] Université Paris-Saclay, 3Joliot Curie, 91190, Gif-sur-Yvette, France
[d] Institute of Low Temperature and Structure Research, Polish Academy of Sciences, Okolna 2, PL-50422, Wroclaw, Poland

ARTICLE INFO

Keywords:
YAG
Substitution effects
Sol-gel synthesis
Optical properties

ABSTRACT

In this study the novel garnet-type $Y_{2.47}Na_{0.5}Ln_{0.03}Al_5O_{12}$, $Y_{2.97}Ln_{0.03}Al_{4.95}V_{0.05}O_{12}$, $Y_{2.92}Na_{0.05}Ln_{0.03}Al_{4.9833}V_{0.0167}O_{12}$ (Ln = Ce^{3+}, Tb^{3+}, Eu^{3+}) phosphors were successfully synthesized by the sol-gel method for the first time. The structural, morphological and optical properties were characterized by using multiple characterization techniques. The XRD and FTIR results confirmed that all obtained phosphors are monophasic yttrium aluminium garnet compounds, i.e. the doping of Ce^{3+}, Tb^{3+}, Eu^{3+}, Na^{+}, V^{5+} ions does not induce any impurity phases, indicating the successful incorporation of these dopants into the YAG host. The formation of novel garnets was probed using ^{27}Al, ^{51}V, ^{23}Na MAS NMR techniques. SEM micrographs revealed that almost in all cases, the surface of the obtained luminophores is porous and consists of homogeneously distributed irregular sphere-like shape particles, which tend to form larger agglomerates. The optical properties of obtained compounds were also investigated by recording their excitation and emission spectra and calculating the colour coordinates in the CIE 1931 colour space.

1. Introduction

In this digital age, increasing energy demand and efforts to combat climate change require the development of new technologies and efficient multifunctional materials. It is also essential to provide environmentally friendly lighting technology and properly select high-efficiency phosphors, which would be able to give good visible light emission. To achieve these goals, there is no better option than solid state lighting [1,2]. Solid state lighting is being popularized rapidly due to its advantages comparing with other traditional lighting sources, especially high efficiency, low energy consumption, durability, less pollution, and long service time [1,3].

Scientists pay special attention to inorganic luminescent materials (luminophores, phosphors), which are practically used in almost all artificial light devices, such as cathode ray tubes, LED, field emission displays. Luminophores are composed of an inert host lattice and an optically excited activator, typically lanthanide or transition metal ions [4]. There are several well-known examples of phosphor host materials, like Y_2O_3, $Gd_3Ga_5O_{12}$, Zn_2SiO_4, $SrAl_2O_4$, $Bi_4Ge_3O_{12}$, $CaAl_2O_4$ [4–7]. Out of them all garnet-type compounds have been recognized as one of the best optical host materials [8,9].

Yttrium aluminium garnet ($Y_3Al_5O_{12}$, YAG) is the representative garnet and widely used in various applications due to its unique properties, such as good optical transparency from ultraviolet to infrared, excellent thermal and chemical stability [9–12]. What is more, high molar part of trivalent rare earth ions can be introduced into the YAG structure by changing Y^{3+} ions without concentration quenching. This feature contributed to the fact, that YAG doped with lanthanides or transition metal ions is the main component in all-colour phosphors, solid-state lasers, scintillators, and vacuum fluorescent displays [4,9,13–15]. For example, europium-doped YAG is the common red phosphor, which characterized by a high quantum efficiency, sufficient absorption strength and stability [16]. This phosphor is used in field emission displays, cathode ray tubes and as fluorescence thermometry due to its optical properties depending on the temperature [6,17]. Cerium-doped YAG is a yellow phosphor with absorption in the blue region and the important component of white light emitting diodes (wLEDs). YAG:Ce^{3+} luminophore shows a high luminescence quantum

* Corresponding author.
E-mail address: aivaras.kareiva@chgf.vu.lt (A. Kareiva).

https://doi.org/10.1016/j.omx.2024.100300
Received 21 November 2023; Received in revised form 15 January 2024; Accepted 28 January 2024
Available online 16 February 2024

yields, good chemical stability and photostability, and already are used commercially [8,13,18,19]. YAG doped with terbium ions is a green phosphor with a narrow emission band suitable for CRT colour projection [20,21].

It is well established, that the optical properties of luminescent materials depend on the doping ions and their concentrations, the crystal structure and chemical composition of the inert phosphor host. For example, doping YAG with big amount of vanadium ions leads to the appearance of impurity phase of YVO_4. It was shown, that the secondary phase of YVO_4 in YAG matrix doped with europium and vanadium improve optical properties, emission intensity was higher in comparison with undoped YAG:Eu^{3+} [22]. To the best of our knowledge, there are no reports regarding the investigation of photoluminescence properties of sodium doped YAG. On the other hand, replacing Y^{3+} ions with lower oxidation state ions, like Ca^{2+}, can lead to the emission intensity increase in praseodymium-doped YAG [23]. Modification of the optical materials matrix is an effective way to obtain luminophores with the new properties [9,23]. In this work YAG matrix was modified by substituting yttrium with sodium, cerium, terbium, europium and by substituting aluminium with vanadium.

The main aim of this work was to synthesize novel garnet-type $Y_{2.47}Na_{0.5}Ln_{0.03}Al_5O_{12}$, $Y_{2.97}Ln_{0.03}Al_{4.95}V_{0.05}O_{12}$, $Y_{2.92}Na_{0.05}Ln_{0.03}Al_{4.9833}V_{0.0167}O_{12}$ (Ln = Ce^{3+}, Tb^{3+}, Eu^{3+}) luminescent materials by the aqueous sol-gel method and to characterize their structural, morphological and optical properties. Several characterization techniques, like X-ray diffraction (XRD) analysis, Fourier-transform infrared spectroscopy (FTIR), scanning electron microscopy (SEM) and solid-state nuclear magnetic resonance (NMR) were used. The optical properties of sintered compounds were investigated by recording their excitation and emission spectra and calculating the colour coordinates in the CIE 1931 colour space. It is important to note, that luminophores with these chemical compositions were synthesized for the first time.

2. Experimental

2.1. Materials

Yttrium nitrate hexahydrate ($Y(NO_3)_3{\cdot}6H_2O$, Alfa Aesar, 99.9 %), aluminium nitrate nonahydrate ($Al(NO_3)_3{\cdot}9H_2O$, Carl Roth, 98 %), sodium acetate (CH_3COONa, Carl Roth, 99 %), ammonium monovanadate (NH_4VO_3, Carl Roth, 99.8 %), trisodium monovanadate (Na_3VO_4, Carl Roth, 99 %), europium(III) oxide (Eu_2O_3, Alfa Aesar, 99.996 %), terbium (III) nitrate pentahydrate ($Tb(NO_3)_3{\cdot}5H_2O$, Aldrich, 99.9 %), cerium(III) nitrate hexahydrate ($Ce(NO_3)_3{\cdot}6H_2O$, Alfa Aesar, 99.99 %) were used as starting materials and citric acid ($C_6H_8O_7$, Chempur, 99.7 %) as a complexing agent.

2.2. Synthesis

An aqueous sol-gel method was used to synthesize the $Y_{3-x}Na_xAl_5O_{12}$, $Y_3Al_{5-y}V_yO_{12}$, $Y_{3-x}Na_xAl_{5-y}V_yO_{12}$, $Y_{2.97}Ln_{0.03}Al_5O_{12}$, $Y_{2.47}Na_{0.5}Ln_{0.03}Al_5O_{12}$, $Y_{2.97}Ln_{0.03}Al_{4.95}V_{0.05}O_{12}$, $Y_{2.92}Na_{0.05}Ln_{0.03}Al_{4.9833}V_{0.0167}O_{12}$ garnets with various stoichiometry. Nominal synthesis was performed to obtain 1 g of the final material. Firstly, stoichiometric amounts of precursors were dissolved in 50 mL of distilled water. Only europium(III) oxide was firstly dissolved in a small amount of concentrated nitric acid at 100 °C and then added to the beaker with the other starting materials. The solution was stirred at 80 °C for 2 h in a beaker covered with a watch-glass. Then, the complexing agent - citric acid (molar ratio metals:citric acid = 1:1) was added to this transparent solution of the metal salts. The mixture was left to mix in a covered beaker, and at this stage a sol was formed. After 24 h, the beaker was uncovered, and the solution was concentrated by the evaporation at 200 °C under constant stirring until the transparent sol turned into sticky gel. The gel was placed into the drying oven at 150 °C for 10 h. Next, the obtained xerogel was grounded in an agate mortar and annealed in air at 1000 °C for 2 h, with the heating rate speed – 5 °C/min. Finally, synthesized garnets were ground in an agate mortar. The simplified scheme of the sol-gel route used is presented in Fig. 1.

2.3. Characterization

X-ray powder diffraction (XRD) analysis (step width of 0.01°, scan speed 5°/min) on Rigaku MiniFlex II diffractometer using Cu K α1 radiation was used to study the phase purity and crystallinity of synthesized samples. The diffraction data was refined by the Rietveld method using the Fullprof suite. For the infrared (IR) spectroscopy measurements Bruker Alpha FTIR spectrometer was used. Solid-state NMR experiments were carried out at 14.1 T on a Bruker Avance Neo 600 NMR spectrometer operating at 156.4 MHz, 158.8 MHz, 157.8 for ^{27}Al, ^{23}Na, ^{51}V, respectively, using a 2.5 mm Trigamma MAS probe. Temperature was stabilized at 298 K and MAS rate was set to 20–30 kHz. All 1D measurements were performed with single pulse excitation, 90° excitation pulse was set to 2.2 μs for ^{27}Al, ^{51}V and 3.5 μs for ^{23}Na. For ^{27}Al spectra 256–512 scans, for ^{51}V 10240–15416 scans, for ^{23}Na 1280–3088 scans were accumulated using a repetition delay of 5 s. For ^{27}Al MQMAS measurements 132 scans for 128 increments were accumulated, the excitation, conversion and selective pulses were set to 4.5 μs, 1.7 μs and 50 μs, respectively. Scanning electron microscope (SEM) images were taken for the morphology characterization using a Hitachi SU-70. The particle size measurements were done using open-source Fiji (ImageJ) software by selecting few hundred random particles. Excitation and emission spectra of the lanthanide-doped samples were recorded on Edinburgh Instruments FLS980 spectrometer equipped with a 450 W Xe arc lamp. The photoluminescence emission spectra were corrected using correction file obtained from a tungsten incandescent lamp certificated by the National Physics Laboratory (UK). Emission spectra of samples doped with Ce^{3+} ions were recorded under 450 nm excitation, doped with Tb^{3+} ions – under 272 nm excitation, and doped with Eu^{3+} ions – under 393.5 nm excitation. The excitation spectra of samples doped with Ce^{3+} ions were measured under 560 nm emission, doped with Tb^{3+} ions – under 542 nm emission, and doped with Eu^{3+} ions – under 589 nm emission. Colour coordinates in CIE 1931 colour space diagrams were calculated from emission spectra employing the Edinburgh Instruments F980 software.

3. Results

3.1. XRD analysis

The phase purity and compositional changes of the YAG doped with different amount of sodium and vanadium were controlled by the XRD analysis. Fig. 2a shows the XRD patterns of the $Y_{3-x}Na_xAl_5O_{12}$ samples sintered at 1000 °C, with the different substitutional level of Na for Y ($0.01 \leq x \leq 2$) in the compounds. The XRD patterns of $Y_{3-x}Na_xAl_5O_{12}$ samples with x = 0.01, 0.05, 0.1, 0.15, 0.3, 0.5, 1 exhibit the formation of single garnet phase, since they are in a good agreement with the reference data for YAG [PDF #96-152-9038]. However, the XRD patterns of $Y_{3-x}Na_xAl_5O_{12}$ with higher amount of sodium (x = 1.5 and 2) contain an additional low-intensity lines of extraneous phases as the perovskite $YAlO_3$ ($2\theta \approx 24.4°$, 34.6°, 45.8°) and aluminium oxide Al_2O_3 ($2\theta \approx 30.2°$, 58°, 66.7°).

The effect of vanadium ions substitution was investigated in $Y_3Al_{5-y}V_yO_{12}$ ($0.01 \leq y \leq 3$) samples. As can be seen from Fig. 2b the monophasic garnet product was only obtained in XRD patterns of $Y_3Al_{4.99}V_{0.01}O_{12}$ and $Y_3Al_{4.95}V_{0.05}O_{12}$, where all observed diffraction peaks match very well the standard XRD data of pure YAG (PDF #96-152-9038). However, in the case of $Y_3Al_{5-y}V_yO_{12}$ with higher introduced amount of vanadium (y = 0.1, 0.15 and 0.3) the formation of the yttrium orthovanadate YVO_4 [PDF #96-901-1138] impurity phase along with the main YAG phase was also determined.

The effect of co-substitution with sodium instead of yttrium and vanadium instead of aluminium was investigated and Fig. 2 c demonstrates

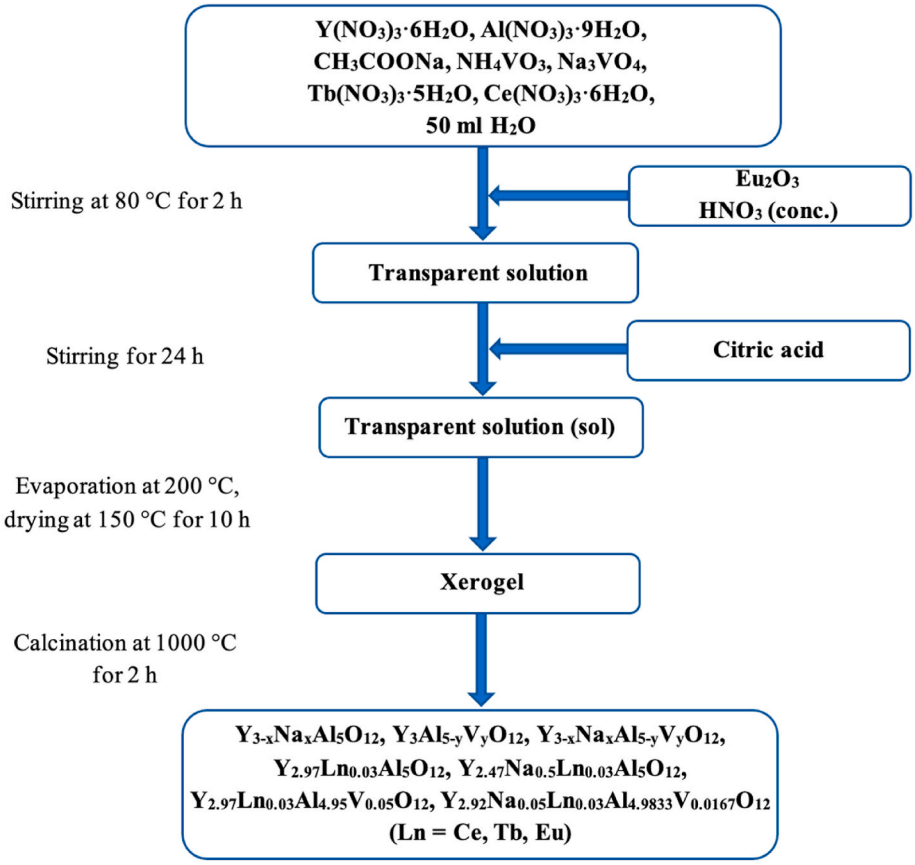

Fig. 1. Scheme of sol-gel synthesis of garnets with various chemical compositions.

the XRD patterns of the $Y_{3-x}Na_xAl_{5-y}V_yO_{12}$ ($0.01 \leq x \leq 0.3$ and $0.0033 \leq y \leq 0.1$) samples. It can be observed that $Y_{2.99}Na_{0.01}Al_{4.9967}V_{0.0033}O_{12}$, $Y_{2.95}Na_{0.05}Al_{4.9833}V_{0.0167}O_{12}$, $Y_{2.9}Na_{0.1}Al_{4.9667}V_{0.0333}O_{12}$ products are crystalline monophasic compounds having a YAG garnet structure. With increasing the molar part of doped ions, the YAG is still the main phase, but additional peaks characteristic to the extraneous YVO_4 [PDF #96-901-1138] and Al_2O_3 [PDF #96-100-0443] phases have appeared.

According to these XRD results presented in Fig. 2a-c, the range of $0.01 \leq x \leq 1$ can be ascribed as the limit of the molar part of sodium in $Y_{3-x}Na_xAl_5O_{12}$ and the narrow range of $0.01 \leq y \leq 0.05$ as the limit of the molar part of vanadium in $Y_3Al_{5-y}V_yO_{12}$. Furthermore, the formation of monophasic co-doped $Y_{3-x}Na_xAl_{5-y}V_yO_{12}$ can be possible, when the substitutional levels of sodium and vanadium are in the range of $0.01 \leq x \leq 0.1$ and $0.0033 \leq y \leq 0.0333$, respectively. Thus, these matrices with novel chemical compositions can successfully be used as optical host materials.

Fig. 2 also shows the XRD patterns of lanthanide-doped $Y_{2.97}Ln_{0.03}Al_5O_{12}$, $Y_{2.47}Na_{0.5}Ln_{0.03}Al_5O_{12}$, $Y_{2.97}Ln_{0.03}Al_{4.95}V_{0.05}O_{12}$, $Y_{2.92}Na_{0.05}Ln_{0.03}Al_{4.9833}V_{0.0167}O_{12}$ garnets, there Ln = Ce (d), Tb (e), Eu (f), sintered by sol-gel method at 1000 °C. All obtained XRD patterns are almost identical and show perfect fit with the standard data of pure YAG [PDF #96-152-9038]. The XRD results confirm, that all lanthanide-doped samples are crystalline single-phase compounds with cubic garnet structure. The diffraction peaks of samples doped with cerium and terbium ions, compared to those of standard data, have a slight shift towards the smaller 2-theta values. An apparent shift can be observed due to the doping of Ce^{3+} and Tb^{3+} with larger ionic radii (1.14 Å and 1.18 Å) compared to that of Y^{3+} (1.019 Å) [19,24]. Since Na^+ and V^{5+} have different oxidation states than Y^{3+} and Al^{3+} ions (the ionic radius for Na^+ is 1.18 Å, and ionic radii for V^{5+} 0.54 Å and for Al^{3+} 0.535 Å are very similar), the introduction of sodium and vanadium should lead to more expressed changes in diffraction peaks positions, which is not the case for our samples. One possible explanation could be that our YAG is considered to be Al_2O_3-rich due to the Na^+ having lower oxidation state than Y^{3+}, which potentially leads to the formation of oxygen vacancies. These effects were observed for non-stoichiometry yttrium aluminium garnet ceramics prepared via solid-state reaction under vacuum [25]. Consequently, the doping of Ce^{3+}, Tb^{3+}, Eu^{3+}, Na^+, V^{5+} ions does not induce any impurity phases, indicating the successful incorporation of these dopants into the YAG host and formation of monophasic garnet-type phosphors. The calculated cell parameters were in the range of 12.012(4)-12.023(3) Å without any tendency upon substitutional level. This probably is related with rather low concentration of substituents.

3.2. FTIR analysis

For the additional structural characterization of doped garnets, the FTIR spectroscopy was utilized. IR spectra of all investigated samples were identical, so Fig. S1 shows the FTIR spectra of the representative specimens. In all IR spectra, the characteristic absorption bands in the higher wavenumbers (from 4000 to 900 cm^{-1}) related to organic groups were not determined which suggests that all organic compounds were evaporated during synthesis and calcination [17,26,27]. It is well established, that the peaks located below 900 cm^{-1} are corresponded to the vibrations of metal-oxygen bonds [27]. In our case, in all obtained IR spectra the broad band in the range from 900 to 400 cm^{-1} is split into several smaller peaks. According to the literature, the peaks at ~423 cm^{-1}, ~450 cm^{-1}, ~568 cm^{-1}, ~721 cm^{-1} correlate to the Y–O (metal-oxygen) vibrations in YAG lattice while the peaks at ~686 cm^{-1} and ~788 cm^{-1} are the characteristic vibrations of the isolated (AlO_4) tetrahedral and (AlO_6) octahedral units in garnet lattice [17,20,27–29]. This feature of the IR spectrum proves the formation of the YAG garnet structure. Thus, the FTIR results are in a good agreement with the XRD

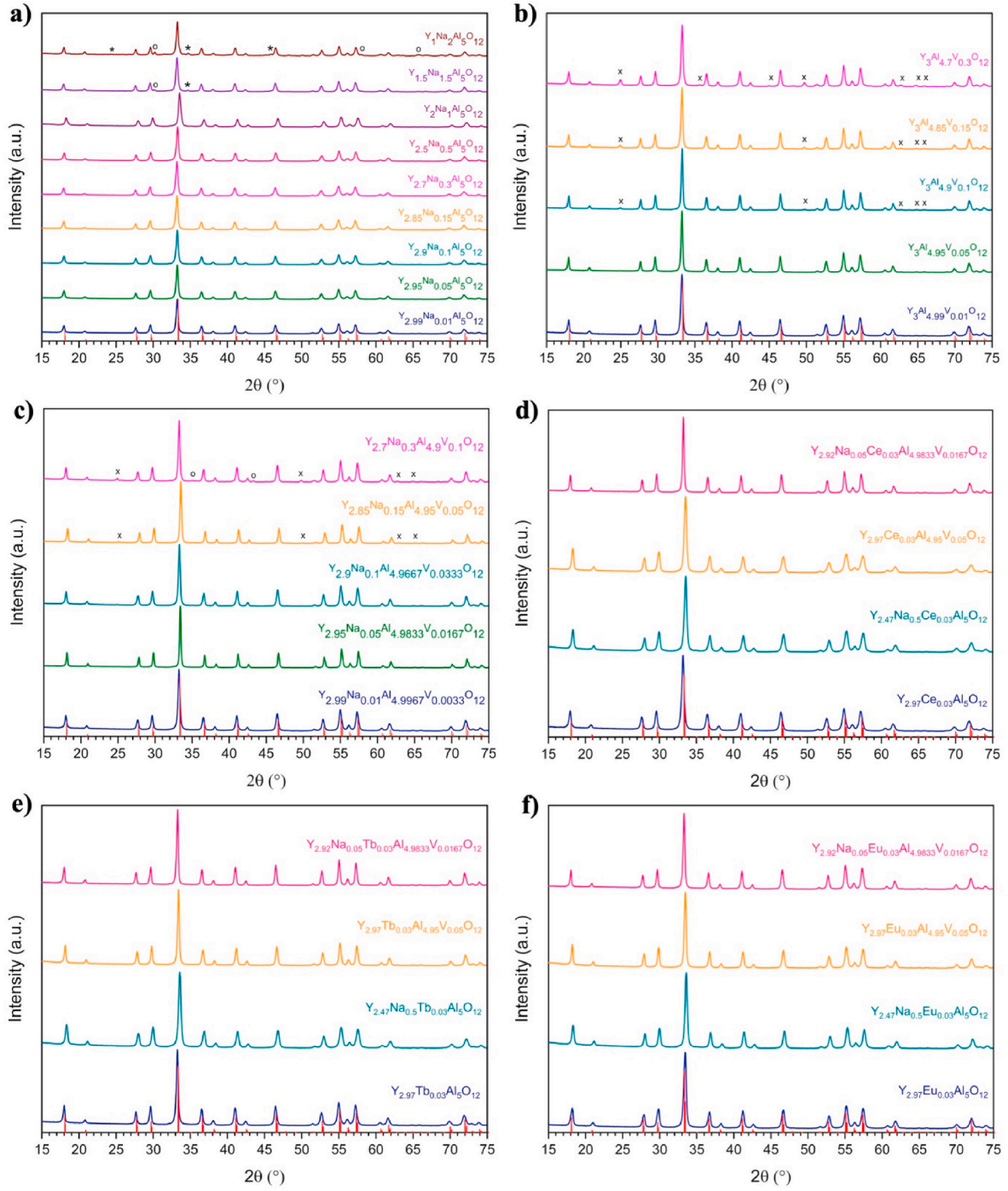

Fig. 2. XRD diffraction patterns of $Y_{3-x}Na_xAl_5O_{12}$ (a), $Y_3Al_{5-y}V_yO_{12}$ (b), $Y_{3-x}Na_xAl_{5-y}V_yO_{12}$ (c) and various stoichiometric YAG doped with Ce^{3+} (d), Tb^{3+} (e), Eu^{3+} (f) samples synthesized at 1000 °C. The crystalline phases are marked: vertical red lines - $Y_3Al_5O_{12}$ [PDF #96-152-9038], * - $YAlO_3$ [PDF #96-153-3070], o - Al_2O_3 [PDF #96-100-0443], x - YVO_4 [PDF #96-901-1138].

results and confirm the fact, that all samples are garnet-type materials.

3.3. Solid state NMR analysis

Solid state NMR analysis was performed for all synthesized samples. Stoichiometric YAG sample possess two spectral lines attributed to sixth-coordinated species (narrow line at 0 ppm) and fourth-coordinated species (quadrupole line at 77.5 ppm, $C_Q = 6095$ kHz and $\eta = 0$) [30]. ^{27}Al NMR signals in YAG-based samples are sensitive probes to detect dopants in close vicinity, namely clear chemical shift change is detected upon changing sample composition [31,32]. The ^{27}Al and 23Na MAS spectra obtained for $Y_{3-x}Na_xAl_5O_{12}$ family of samples are shown in Fig. 3.

Upon doping the samples with Na ions in addition to typical lines detected for YAG samples (sixth-coordinated and fourth-coordinated) the line attributed to AlO_6:Na (six coordinated Al line with Na in vicinity) appears at 8.5 ppm in ^{27}Al spectra. When $x \geq 1$, additional side phases are detected in the spectra, namely spectral lines attributed to Al_2O_3 at 67 ppm, 13.5 ppm, sodium aluminates at 76 ppm and perovskite-like species (YAP, $YAlO_3$) at 0.2 ppm [33,34]. Such assignment is in agreement with the XRD data.

As well such assignment is corroborated by ^{27}Al 3Q MQMAS data

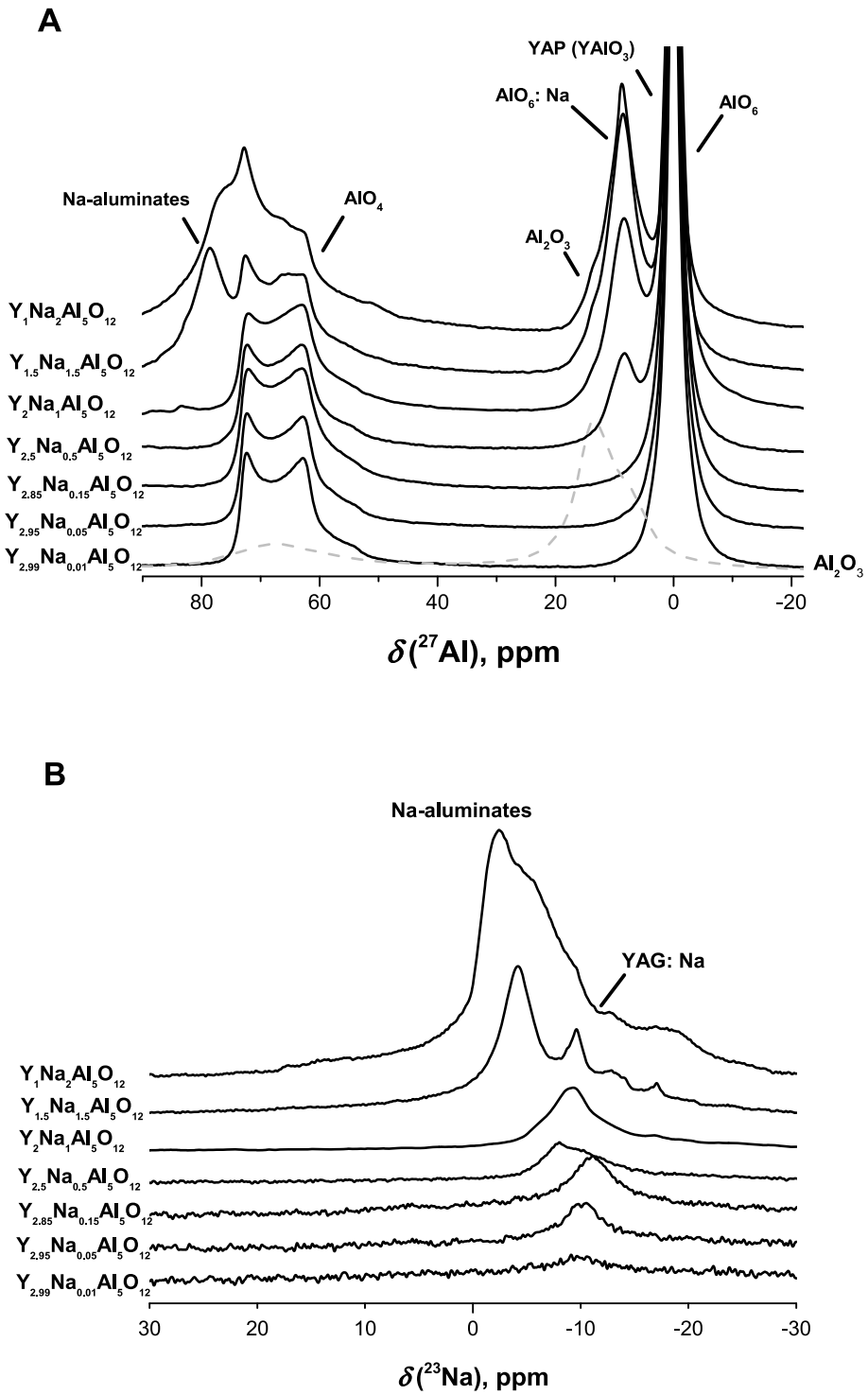

Fig. 3. A – ^{27}Al 30 kHz MAS NMR spectra obtained for $Y_{3-x}Na_xAl_5O_{12}$ samples, Al_2O_3 spectrum is shown in grey dashed line. B – 20 kHz ^{23}Na MAS NMR spectra obtained for $Y_{3-x}Na_xAl_5O_{12}$ samples.

obtained for $Y_1Na_2Al_5O_{12}$ sample (Fig. 4 A). In this 2D spectrum species assigned to YAG and YAG:Na species as well as side YAP, Al_2O_3 and sodium aluminates phases are detected. The final spectral fitting which agrees well with the experiment is shown in Fig. 4 B.

^{23}Na data obtained for the $Y_{3-x}Na_xAl_5O_{12}$ family of samples (Fig. 4 B) proves the incorporation of Na ions in the garnet structure and shows the formation of side phases when the amount of Na is higher ($x \geq 1$). The peak assigned to YAG:Na structure is located at 9.5 ppm, other spectral lines likely arise from various sodium aluminate phases, though these were not studied in detail as it was beyond the scope of present work [33,34].

The ^{27}Al and ^{51}V MAS spectra obtained for $Y_3Al_{5-y}V_yO_{12}$ family of samples are shown in Fig. 5. Upon doping the samples with V ions along to the typical lines obtained for YAGs the line attributed to AlO_6:V (six coordinated Al line with V in vicinity) appears at 20.5 ppm in ^{27}Al NMR spectra. Similarly as in the case of Na ion, the line attributed to AlO4:V is not observed most probably due to low intensity and large width of the line. In the ^{51}V NMR data the formation of the YVO_4 (664 ppm) side

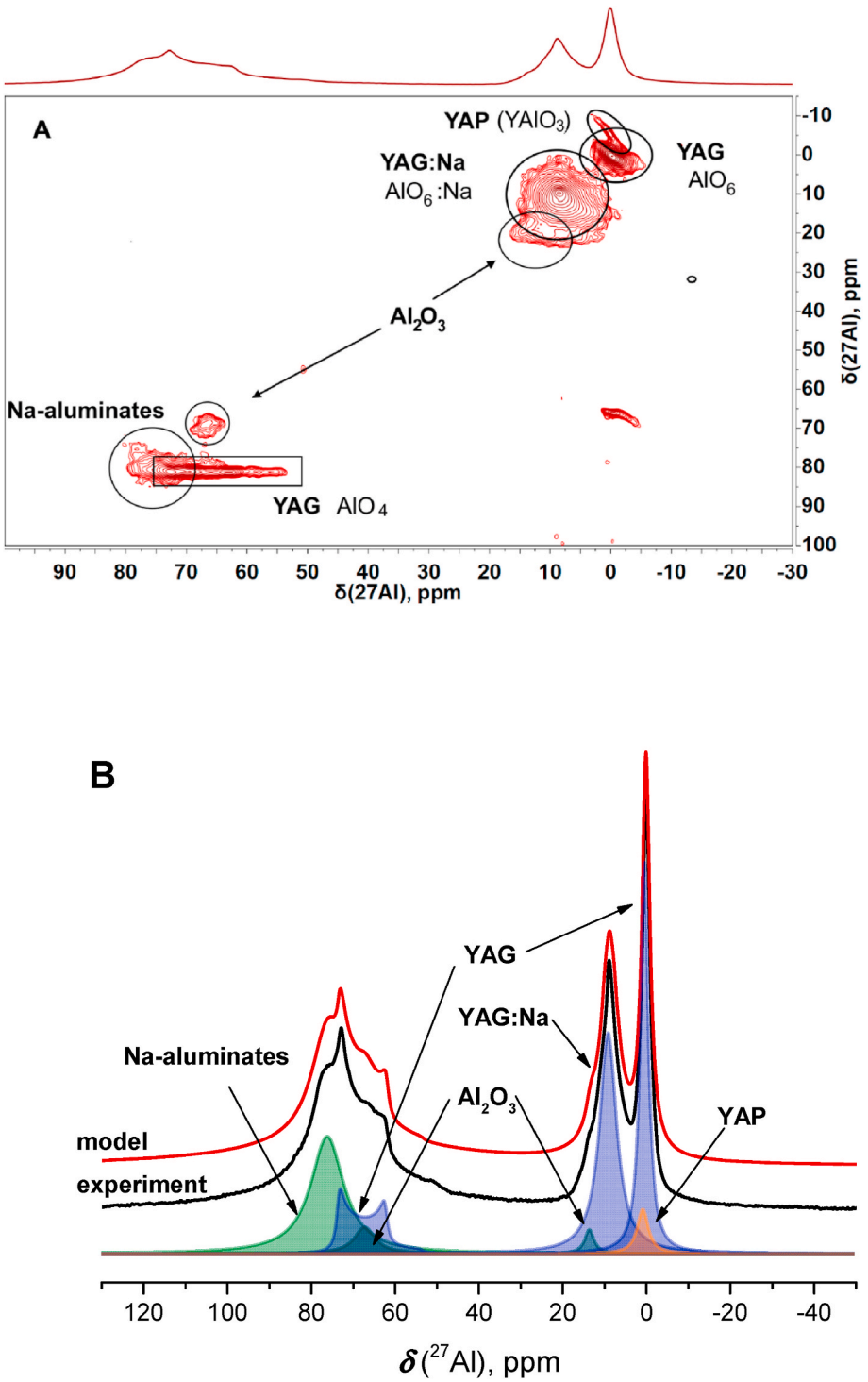

Fig. 4. A – ^{27}Al MQMAS spectrum obtained for $Y_1Na_2Al_5O_{12}$ sample. Signals attributed to ^{27}Al species are indicated with black circles and squares. B – ^{27}Al MAS spectral fitting based on the 3Q MQMAS data. Black line – experimental data, red line – spectral fitting, orange – YAP phase, blue – YAG and YAG:Na phases, green – Al_2O_3 phase and Na aluminates.

phase is detected when y $\geq$ 0.1 [35]. Though, the line attributed to garnet structure is not observed which could be due to low amount of ^{51}V species as well as the line is likely broad and vanishes within the noise or spin-spin relaxation T_2 is too fast for detection.

The ^{27}Al, ^{23}Na and ^{51}V MAS spectra obtained for $Y_{3-x}Na_xAl_{5-y}V_yO_{12}$ family of samples are shown in Fig. 6. The ^{27}Al NMR spectra upon doping with Na and V ions features the same tendencies as upon doping YAGs with Na and V ions separately, namely lines attributed to AlO_6:Na at 13.5 ppm and AlO_6:V at 20.5 ppm appears. In ^{23}Na MAS spectrum the line attributed to YAG: Na species is at −13 ppm and the line at −25 ppm is attributed to $NaAlO_2$ [36]. In the ^{51}V MAS spectra the line attributed to YAG: V species at 575 ppm increases upon doping with V ions. Similarly, as before the YVO_4 side phase which line is at 663 ppm is formed at higher V concentrations. It is seen from the solid state NMR data that co-doping with V and Na ions allows to form more homogenous garnet samples. In particular, ^{51}V and ^{23}Na MAS NMR is sensitive to probe species which are not detected indirectly via ^{27}Al MAS NMR.

^{27}Al MAS NMR spectra obtained for the Ce, Eu, Tb doped $Y_{3-x}Na_xAl_{5-}$

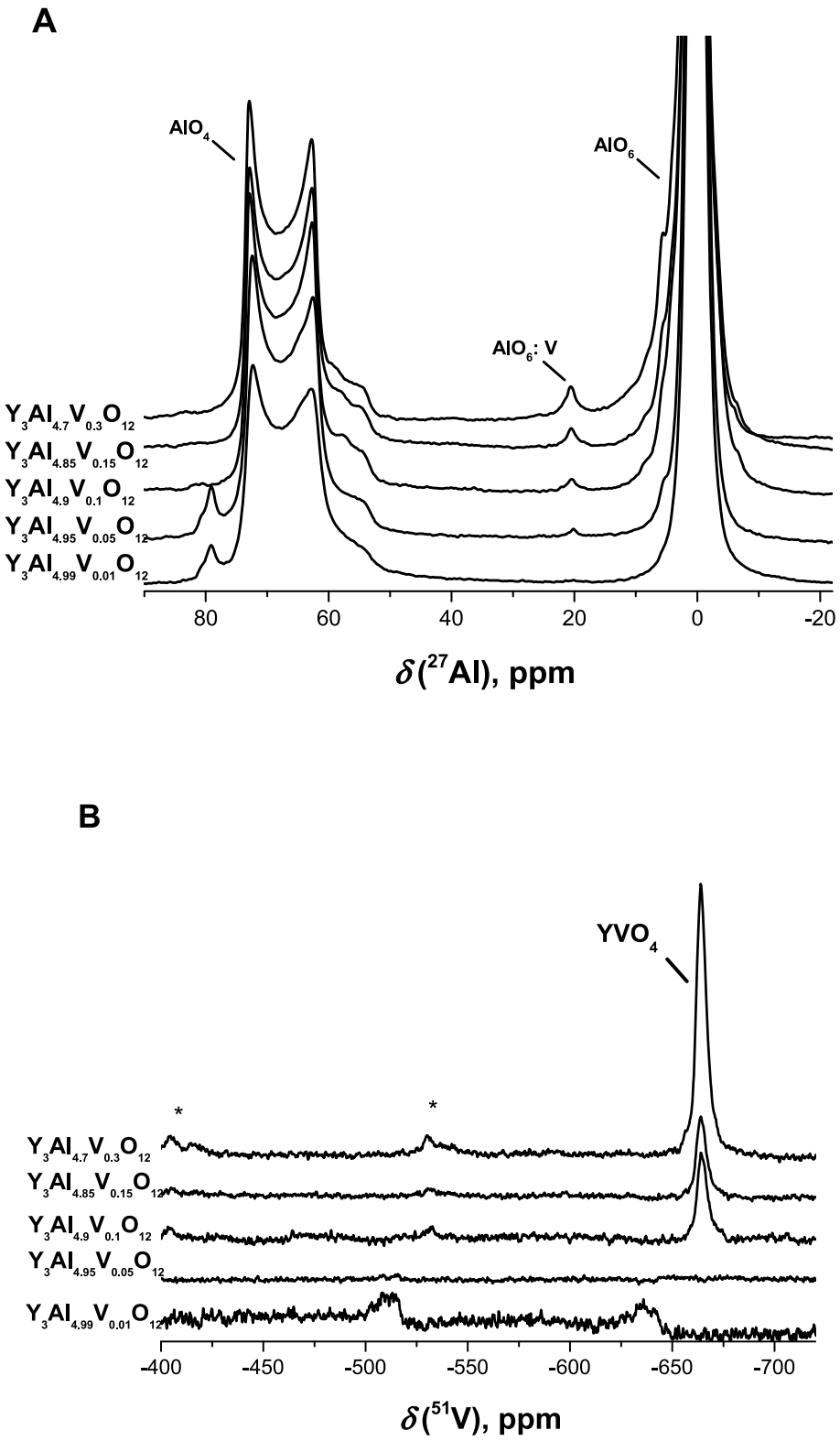

Fig. 5. A – ^{27}Al 30 kHz MAS NMR spectra obtained for $Y_3Al_{5-y}V_yO_{12}$ samples. B – 20 kHz ^{51}V MAS NMR spectra obtained for $Y_3Al_{5-y}V_yO_{12}$ samples.

$_yV_yO_{12}$ samples are shown in Fig. 7. The tendencies observed in the spectra upon doping the garnet samples with Na and V ions are the same as discussed before, namely the associated spectral lines with AlO_6:Na and AlO_6:Na species are detected in the same spectral regions. In addition, the lines associated to AlO_6:Ce (Fig. 7 A) at −17.5 ppm, AlO_6:Eu (Fig. 7 B) at 114 ppm species are detected. The detected ^{27}Al chemical shift values when Ce or Eu are in a vicinity to AlO_6 units are similar to previously detected values [31,37]. The line attributed to AlO_6:Tb (Fig. 7C) is not detected directly in ^{27}Al NMR spectra due to paramagnetic nature of Tb ion. The estimated value for such species should be at ca. 500 ppm [37] but was not detected before studying YAG:Tb samples [38]. Nevertheless, the increase of the linewidths in ^{27}Al NMR

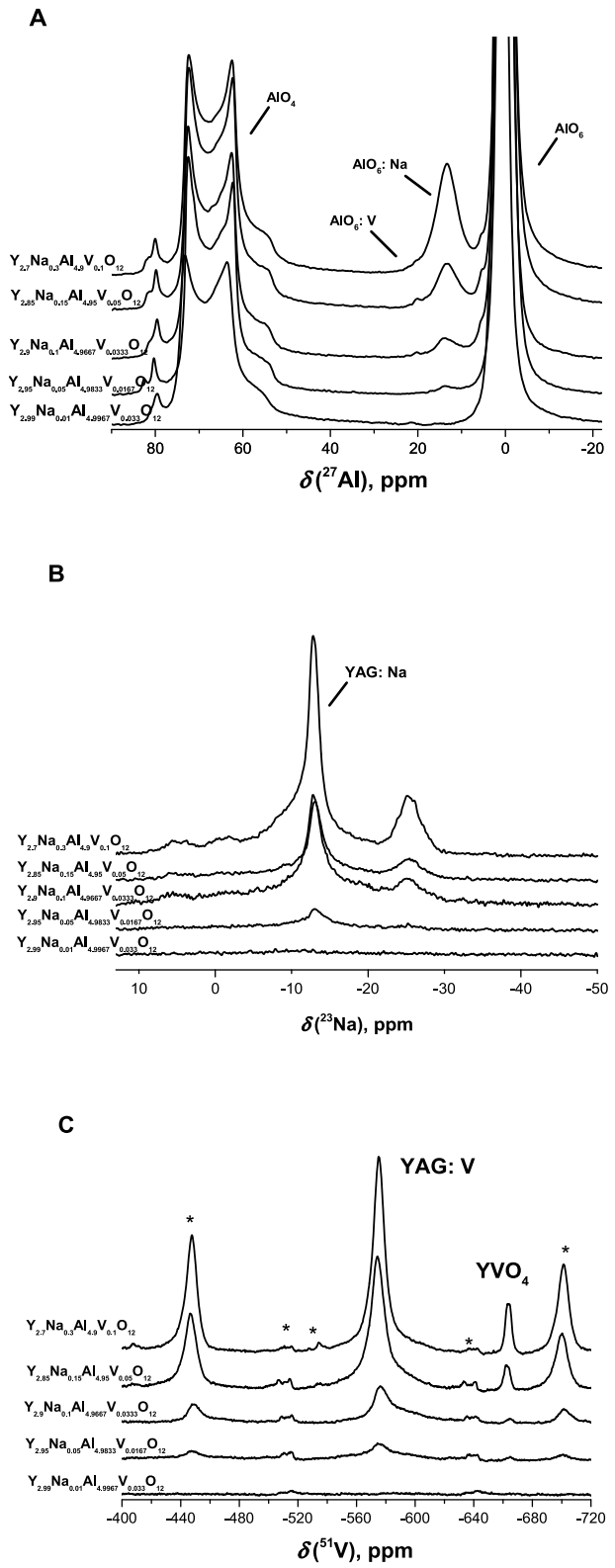

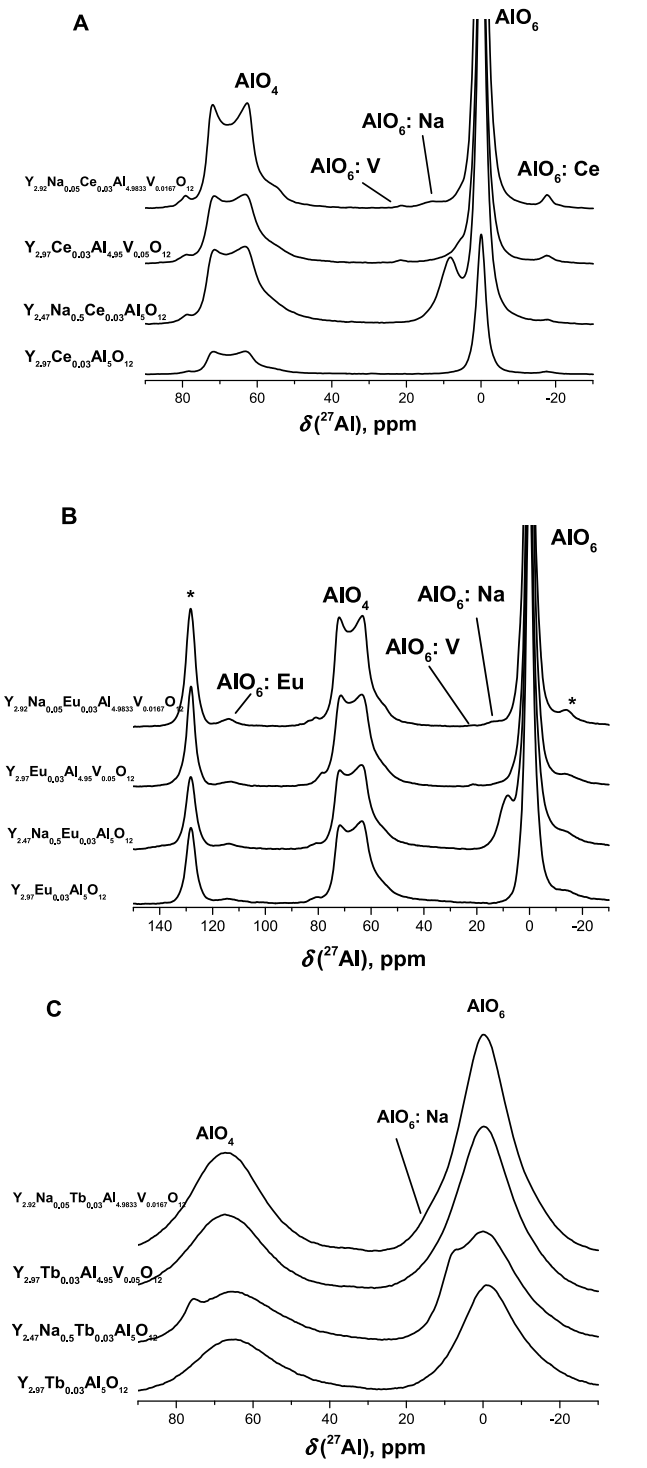

Fig. 6. A – ^{27}Al 30 kHz MAS NMR spectra obtained for $Y_{3-x}Na_xAl_{5-y}V_yO_{12}$ samples. B – 20 kHz ^{23}Na MAS NMR spectra obtained for $Y_{3-x}Na_xAl_{5-y}V_yO_{12}$ samples. C – 20 kHz ^{51}V MAS NMR spectra obtained for $Y_{3-x}Na_xAl_{5-y}V_yO_{12}$ samples.

spectra indirectly indicates successful incorporation of Tb ions in the garnet structure. The obtained NMR data allows us to state that the proposed garnet structures were successfully synthesized and the incorporation of Ce, Eu, Tb ions were successful.

Fig. 7. ^{27}Al 20 kHz MAS NMR spectra obtained for $Y_{3-x}Na_xAl_{5-y}V_yO_{12}$ samples doped with A – Ce, B–Eu, C–Tb ions.

3.4. SEM analysis

All specimens were characterized by scanning electron microscopy to investigate their surface morphology, porosity, and particle size. From the obtained SEM results it was determined that all lanthanide-doped samples have very similar surface morphology, therefore Fig. 8 shows europium-doped YAG with various compositions as a representative. SEM micrographs of the $Y_{2.97}Eu_{0.03}Al_5O_{12}$ (a), $Y_{2.47}Na_{0.5}Eu_{0.03}Al_5O_{12}$ (b) and $Y_{2.97}Eu_{0.03}Al_{4.95}V_{0.05}O_{12}$ (c) phosphors demonstrate, that specimens are homogeneous with a porous surface.

The formation of pores can occur due to escaping gases during the calcination process. As we can see from Fig. 9 the surface porosity decreases, when YAG is doped with sodium or vanadium. Interestingly, the number of pores is smaller, when YAG is doped with sodium in comparison with vanadium. Furthermore, doping YAG with both sodium and vanadium ions leads to minimal number of pores. Three samples, namely $Y_{2.97}Eu_{0.03}Al_5O_{12}$ (Fig. 8a), $Y_{2.47}Na_{0.5}Eu_{0.03}Al_5O_{12}$ (Fig. 8b) and $Y_{2.97}Eu_{0.03}Al_{4.95}V_{0.05}O_{12}$ (Fig. 8c), are composed of irregular sphere-like shape particles, which tend to form larger agglomerates. According to the previous reports, the formation of pores and particle agglomeration are the characteristic morphology features for the samples with garnet structure prepared by sol-gel synthesis method [10,39,40]. When both sodium and vanadium is introduced into YAG, the shape of the particles drastically changes, and particles tend to sinter to larger aggregates. This $Y_{2.92}Na_{0.05}Eu_{0.03}Al_{4.9833}V_{0.0167}O_{12}$ sample consists of grains with explicit grain boundaries (Fig. 8d). Moreover, particle size varies depending on the introduced element. The smallest particles can be observed for the sample doped with 1% of europium, ranging from 10 to 50 nm. The $Y_{2.47}Na_{0.5}Eu_{0.03}Al_5O_{12}$ (Fig. 8b) and $Y_{2.97}Eu_{0.03}Al_{4.95}V_{0.05}O_{12}$ (Fig. 8c) samples have almost identical particle size, which varies from 20 to 90 nm. The particle size significantly increases in the range of 50–200 nm, when YAG is doped with both sodium and vanadium ions.

3.5. Optical properties

The emission and excitation spectra were measured on spectrometer to describe the optical properties of the obtained lanthanide-doped garnets. Fig. 9a shows excitation spectra of cerium-doped YAG with different stoichiometry, recorded at room temperature for the 560 nm emission. Two broad symmetric bands can be seen, which belong to [Xe] $4f^1 \rightarrow$ [Xe]5 d^1 transitions. According to the literature data, this is a typical excitation spectrum of Ce^{3+} ions, where a lower intensity band in the wavelength range of 320–360 nm (maximum at 340 nm) belongs to the $^2F_{5/2} \rightarrow {}^2D_{5/2}$ transition, and a higher intensity peak with a maximum at 455 nm wavelength belongs to the $^2F_{7/2} \rightarrow {}^2D_{3/2}$ transition [16]. It should be noted that the higher energy band is weaker than the lower energy band. Scientists say that this may be caused by photoionization, where higher crystal-field component of the excited [Xe]5 d^1 configuration of Ce^{3+} is in or close to the conduction band [41]. Furthermore, the highest excitation intensity was obtained for $Y_{2.97}Ce_{0.03}Al_5O_{12}$ luminophore and the lowest for – $Y_{2.47}Na_{0.5}Ce_{0.03}Al_5O_{12}$ luminophore.

Fig. 9b presents the corrected emission spectra of the garnets doped with Ce^{3+} ions, recorded under 450 nm excitation. During the emission, the electrons of the excited state [Xe]5 d^1 return to the rest state [Xe]$4f^1$, which, due to the spin-orbit interaction, is split into two levels, i.e. $^2F_{5/2}$ and $^2F_{7/2}$. As a result, a broad asymmetric band is observed in the emission spectrum at a wavelength of 530 nm, and it consists of two strongly overlapping bands, which are attributed to the 5 $d^1 \rightarrow {}^2F_{5/2}$ and 5 $d^1 \rightarrow {}^2F_{7/2}$ transitions [42]. The positions of the bands of the emission spectra shown in Fig. 10b coincide with the characteristic emission of trivalent cerium mentioned in the literature [2,16,42–44]. The emission spectra show the same trend as the excitation spectra: the $Y_{2.97}Ce_{0.03}Al_5O_{12}$ phosphor has the most intensive emission, and the $Y_{2.47}Na_{0.5}Ce_{0.03}Al_5O_{12}$ phosphor has the lowest intensity emission.

The optical properties of compounds doped with Tb^{3+} ions were also studied by recording the emission and excitation spectra of the specimens. Fig. 10a demonstrates the excitation spectra of terbium-doped YAG with various chemical compositions, measured at room temperature for the 542 nm emission. Two broad excitation bands are visible in the spectrum: a higher intensity from 250 to 295 with a maximum at 272 nm and a lower intensity from 310 to 335 with a maximum at 322 nm. The observed bands correspond to the low and high spin [Xe]$4f^8 \rightarrow$ [Xe]$4f^7$5 d^1 transitions of terbium(III) ions [1,42,45]. This is known to be a typical excitation spectrum of Tb^{3+} ions [1,20,42,44–46]. It was also determined, that the $Y_{2.97}Tb_{0.03}Al_5O_{12}$ luminophore has the highest excitation intensity. The excitation intensity of $Y_{2.47}Na_{0.5}Tb_{0.03}Al_5O_{12}$ garnet was also high. In comparison, low and equal excitation intensity is characteristic to $Y_{2.97}Tb_{0.03}Al_{4.95}V_{0.05}O_{12}$ and $Y_{2.92}Na_{0.05}Tb_{0.03}Al_{4.9833}V_{0.0167}O_{12}$ phosphors, so their spectra overlap.

The corrected emission spectra are given in Fig. 10b. These spectra were recorded after excitation of terbium-doped samples with 272 nm radiation. The emission peaks are narrowband and are attributed to electron transitions $^5D_4 \rightarrow {}^7F_j$ and $^5D_3 \rightarrow {}^7F_j$ of the Tb(III) ion [1,44]. Non-intensive transitions are observed in all spectra: $^5D_3 \rightarrow {}^7F_5$ occurs at wavelengths of 370–388 nm with a maximum at 383 nm, $^5D_3 \rightarrow {}^7F_4$ (409–422 nm) with a maximum at 418 nm, $^5D_3 \rightarrow {}^7F_3$ (430–450 nm)

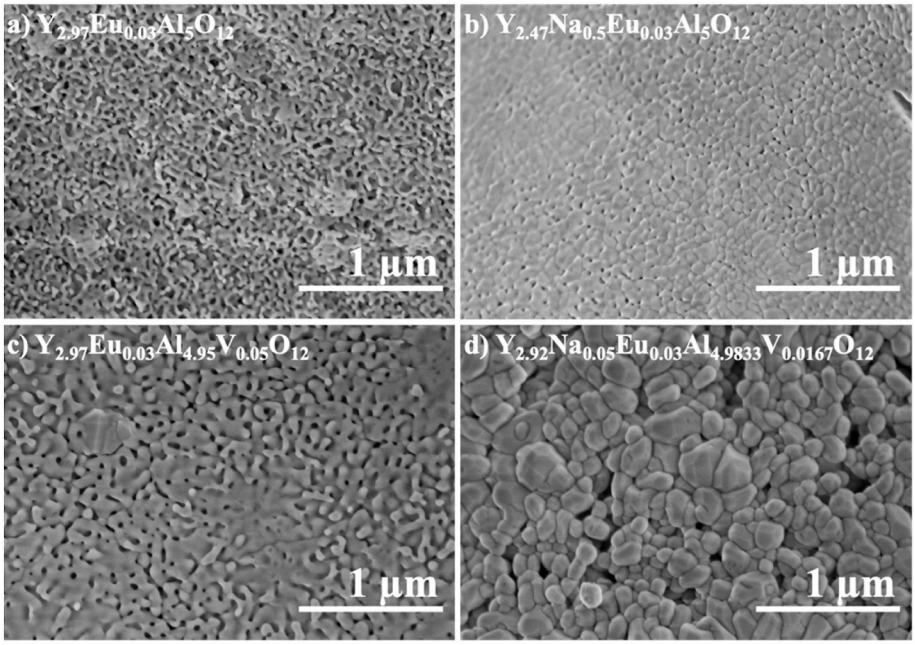

Fig. 8. SEM micrographs of the $Y_{2.97}Eu_{0.03}Al_5O_{12}$ (a), $Y_{2.47}Na_{0.5}Eu_{0.03}Al_5O_{12}$ (b), $Y_{2.97}Eu_{0.03}Al_{4.95}V_{0.05}O_{12}$ (c), $Y_{2.92}Na_{0.05}Eu_{0.03}Al_{4.9833}V_{0.0167}O_{12}$ (d) garnets synthesized at 1000 °C for 2 h.

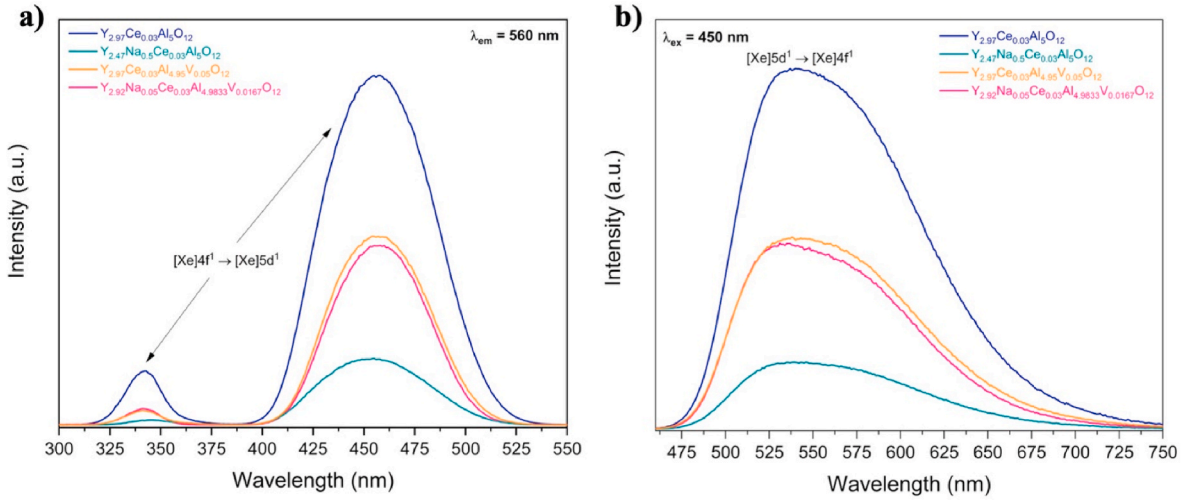

Fig. 9. The excitation(a) and corrected emission(b) spectra of cerium-doped YAG with various chemical compositions.

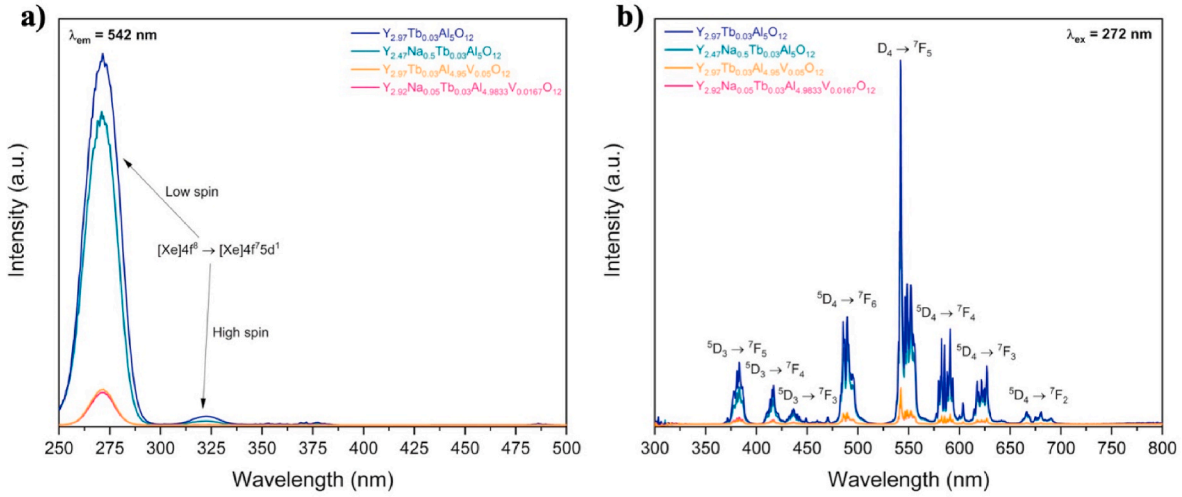

Fig. 10. The excitation(a) and corrected emission(b) spectra of terbium-doped YAG with various chemical compositions.

with a maximum at 438 nm. In the blue region was noticed a higher intensity $^5D_4 \rightarrow {}^7F_6$ transition (480–500 nm) with a maximum at 490 nm. The most intensive peak at 542 nm belongs to the $^5D_4 \rightarrow {}^7F_5$ transition, which is obtained in the green region and gives the green emission colour characteristic to terbium(III) ions. A low intensity $^5D_4 \rightarrow {}^7F_4$ transition (580–608 nm) with a maximum at 591 nm is visible in the orange region. In the red region, a low intensity $^5D_4 \rightarrow {}^7F_3$ transition (614–647 nm) with a maximum at 628 nm and a non-intensive $^5D_4 \rightarrow$

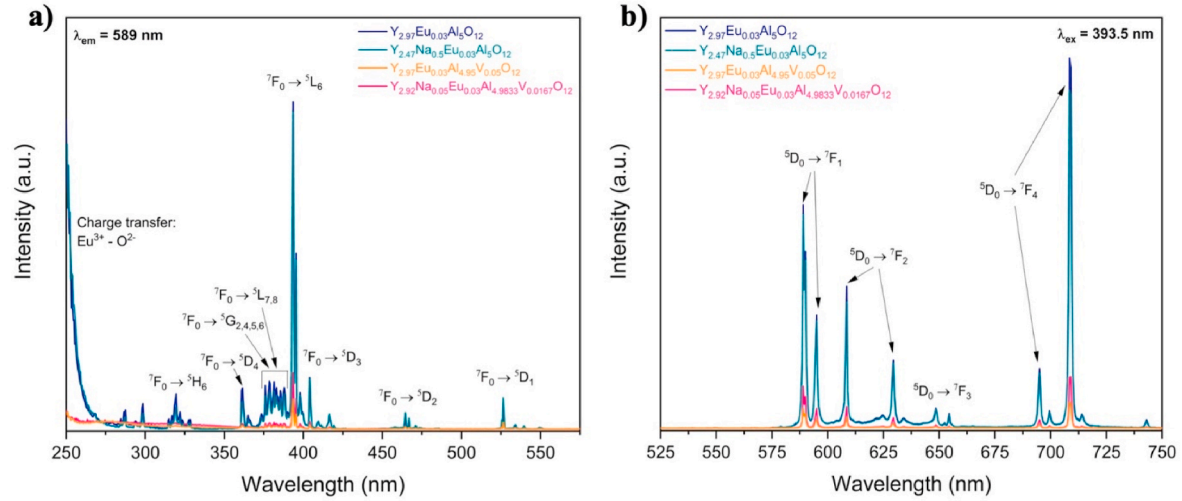

Fig. 11. The excitation(a) and corrected emission(b) spectra of europium-doped YAG with various chemical compositions.

$^7F_2$ transition at 662–693 nm are detected. As it is known from the literature [1,20,42,44,45], these peaks of the emission spectra are attributed to the terbium-doped compounds with YAG garnet structure. In the emission spectra we see the same trend as in the excitation spectra: $Y_{2.97}Tb_{0.03}Al_5O_{12}$ and $Y_{2.47}Na_{0.5}Tb_{0.03}Al_5O_{12}$ phosphors have high and similar magnitude emission intensity, so their emission spectra overlap, while $Y_{2.97}Tb_{0.03}Al_{4.95}V_{0.05}O_{12}$ and $Y_{2.92}Na_{0.05}Tb_{0.03}Al_{4.9833}V_{0.0167}O_{12}$ luminophores have low intensity emission spectra and overlap each other due to their similarities.

Fig. 11a shows the excitation spectra of europium-doped YAG with different compositions, recorded under 589 nm emission. A broad band is observed in the excitation spectra in the wavelength range from 200 to 280 nm, which, according to literature sources [5,6,17,19], is due to charge transfer (CT) between Eu^{3+} and O^{2-} ions and can be described by the following equation: $Eu^{3+} + O^{2-} \rightleftarrows Eu^{2+} + O^-$. The position of this band depends on the coordination number of Eu^{3+} and the covalency of the Eu^{3+} - O^{2-} bond, which is strongly influenced by the nearest Y^{3+} or Al^{3+} cations [6,17]. What is more, transitions of low intensity occur in all spectra: $^7F_0 \rightarrow {}^5D_4$ (363 nm), $^7F_0 \rightarrow {}^5L_{7,8}$ and $^7F_0 \rightarrow {}^5G_{2,4,5,6}$ (370–390 nm), $^7F_0 \rightarrow {}^5D_3$ (405 nm), $^7F_0 \rightarrow {}^5D_1$ (526 nm) and also low intensity $^7F_0 \rightarrow {}^5D_2$ (464 nm) transition. The peak of maximum intensity is seen at the wavelength of 395 nm, which correspond to the $^7F_0 \rightarrow {}^5L_6$ transition. The spectra of $Y_{2.97}Eu_{0.03}Al_5O_{12}$ and $Y_{2.47}Na_{0.5}Eu_{0.03}Al_5O_{12}$ luminophores are characterized by high excitation intensity and are similar, so their peaks overlap. It is interesting to note, that in the spectra of these garnets the $^7F_0 \rightarrow {}^5H_6$ transition with maximum at 320 nm also appeared. The excitation spectra of $Y_{2.97}Eu_{0.03}Al_{4.95}V_{0.05}O_{12}$ and $Y_{2.92}Na_{0.05}Eu_{0.03}Al_{4.9833}V_{0.0167}O_{12}$ garnets have very low intensity and are almost identical, so they overlap with each other.

The corrected emission spectra of samples doped with europium ions are demonstrated in Fig. 11b. Emission spectra were measured under 393.5 nm excitation. All obtained peaks in the emission spectra are attributed to $^5D_0 \rightarrow {}^7F_{1,2,3,4}$ transitions. The magnetic dipole $^5D_0 \rightarrow {}^7F_1$ transition occurs in the wavelength range of 585–596 nm with a high intensity maximum at 588 nm and is characterized by an orange-red colour. The electric dipole $^5D_0 \rightarrow {}^7F_2$ transition occurs in the wavelength range of 606–631 nm with a maximum at 608 nm. It should be noted that the electric dipole transitions are particularly sensitive to the local symmetry of the crystallographic unit in which Eu^{3+} ions are inserted, i.e. the more symmetrical the environment of Eu^{3+} ions, the weaker is the intensity of the electric dipole transition [5,44,47]. Analyzing the emission spectra, we noticed that the intensity of the magnetic dipole $^5D_0 \rightarrow {}^7F_1$ transitions is higher than the intensity of the electric dipole $^5D_0 \rightarrow {}^7F_2$ transition. According to the literature, in the compounds with garnet structure, the Y^{3+} ions occupy dodecahedral positions with D_2 point symmetry [5,11,17]. The D_2 point group is very close to the D_{2h} point group, which has an inversion center, i.e. high symmetry, so the electric dipole $^5D_0 \rightarrow {}^7F_2$ transition in garnet-type materials is strongly suppressed. In addition, in the red region a low intensity $^5D_0 \rightarrow {}^7F_3$ transition (648–655 nm) with a maximum at 649 nm and a high intensity $^5D_0 \rightarrow {}^7F_4$ transition with a maximum at 709 nm are visible. It is interesting to note, that such intensity peaks of the $^5D_0 \rightarrow {}^7F_4$ transition are only observed in garnet structure compounds and lanthanide orthophosphates ($LnPO_4$) [42]. The intensity of the emission lines of $Y_{2.97}Eu_{0.03}Al_5O_{12}$ and $Y_{2.47}Na_{0.5}Eu_{0.03}Al_5O_{12}$ phosphors were practically the same, so the emission spectra of these compounds overlapped. Meanwhile, the intensity of the emission spectra of the $Y_{2.97}Eu_{0.03}Al_{4.95}V_{0.05}O_{12}$ and $Y_{2.92}Na_{0.05}Eu_{0.03}Al_{4.9833}V_{0.0167}O_{12}$ samples was lower than the before mentioned two compounds, but their emission intensity differed little.

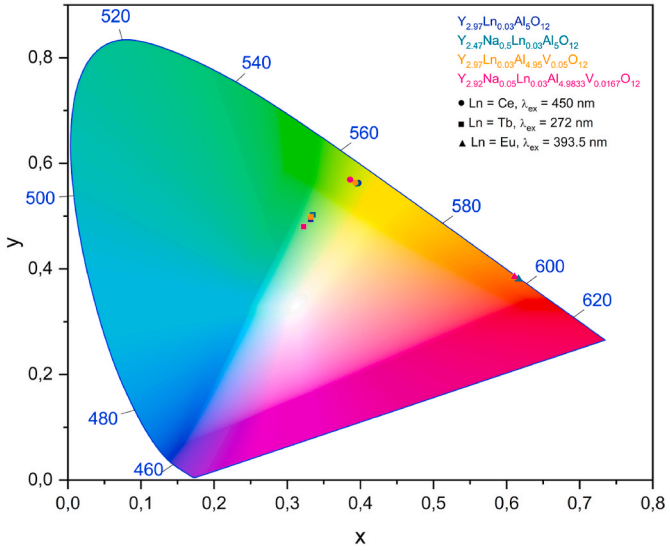

Fig. 12. 1931 CIE chromaticity diagram with points indicating coordinates for $Y_{2.97}Ln_{0.03}Al_5O_{12}$ (blue), $Y_{2.47}Na_{0.5}Ln_{0.03}Al_5O_{12}$ (green), $Y_{2.97}Ln_{0.03}Al_{4.95}V_{0.05}O_{12}$ (orange) $Y_{2.92}Na_{0.05}Ln_{0.03}Al_{4.9833}V_{0.0167}O_{12}$ (pink) phosphors, where ● – Ln = Ce, λ_{ex} = 450 nm, ■ – Ln = Tb, λ_{ex} = 272 nm, ▲ – Ln = Eu, λ_{ex} = 393.5 nm.

The tone and saturation of the emission colour of the synthesized compounds was estimated from the chromaticity coordinates calculated from the emission spectra in the 1931 CIE colour diagram [18]. Fig. 12 shows the CIE 1931 colour diagram with the colour coordinates of garnets doped with cerium(III), terbium(III), europium(III) ions. From the colour diagram, it can be seen, that the emission of Ce^{3+} ions in YAG garnets with various chemical compositions is in the green-yellow region of the visible spectrum, because YAG crystalline structure compounds generate a strong crystalline field [14,15,17]. The colour coordinates of Tb^{3+} ion emission in YAG with different stoichiometric are located in the yellowish-green region of the visible spectrum. The emission of Tb^{3+} ion in $Y_{2.92}Na_{0.05}Tb_{0.03}Al_{4.9833}V_{0.0167}O_{12}$ is significantly shifted towards the blue region of the spectrum compared to other phosphors. Furthermore, the colour coordinates of $Y_{2.47}Na_{0.5}Ce_{0.03}Al_5O_{12}$ and $Y_{2.97}Ce_{0.03}Al_{4.95}V_{0.05}O_{12}$ phosphors, also of $Y_{2.97}Tb_{0.03}Al_5O_{12}$ and $Y_{2.97}Tb_{0.03}Al_{4.95}V_{0.05}O_{12}$ samples overlap due to their x and y values being almost identical. The emission colours of the phosphors doped with Ce(III) ions have high saturation because they are close to the edge of the colour chart, where certain hues are most saturated, while the emission colours of Tb(III) ions in YAG garnets have low saturation because the colour coordinates of the samples are very far from the edge of the colour diagram. In addition, it is obvious that the colour coordinates of all Eu(III)-doped compounds are located right on the edge of the CIE 1931 colour chart in the reddish-orange region of the visible spectrum, indicating a high saturation of the emission colour. What is more, the colour coordinates of all luminophores with europium are very similar, so $Y_{2.97}Eu_{0.03}Al_5O_{12}$ and $Y_{2.47}Na_{0.5}Eu_{0.03}Al_5O_{12}$, also $Y_{2.97}Eu_{0.03}Al_{4.95}V_{0.05}O_{12}$ and $Y_{2.92}Na_{0.05}Eu_{0.03}Al_{4.9833}V_{0.0167}O_{12}$ garnets overlap. On the other hand, such a coincidence of colour coordinates is not surprising, since the emission spectra of the mentioned compounds are almost identical.

4. Conclusions

In this study, the novel $Y_{2.97-x}Ln_{0.03}Na_xAl_{5-y}V_yO_{12}$ (Ln = Ce, Tb, Eu) luminophores were successfully prepared by the sol-gel method heating the obtained gels at 1000 °C for the first time. The maximum substitutions levels for both sodium and vanadium were determined, where the formation of single phase YAG can still occur. For sodium ions, the x can vary from 0.01 up to 1, while in vanadium case, only 0.05 can be introduced. Finally, the suitable matrices for new luminophores were found and doped with lanthanide ions. The XRD and FTIR results confirmed that synthesized $Y_{2.97}Ln_{0.03}Al_5O_{12}$, $Y_{2.47}Na_{0.5}Ln_{0.03}Al_5O_{12}$, $Y_{2.97}Ln_{0.03}Al_{4.95}V_{0.05}O_{12}$, $Y_{2.92}Na_{0.05}Ln_{0.03}Al_{4.9833}V_{0.0167}O_{12}$ products are monophasic yttrium aluminium garnet compounds. Solid state ^{27}Al,

^{51}V, ^{23}Na MAS NMR allowed to probe and monitor the formation of novel type garnets and the obtained data corroborated to the XRD and FTIR data. SEM micrographs revealed that almost in all cases, the surface of the obtained luminophores is porous and consists of homogeneously distributed irregular sphere-like shape particles, which tend to form larger agglomerates. The photoluminescence emission spectra of cerium doped various stoichiometric composition YAG showed the typical Ce^{3+} broad emission peak at ~530 nm due to $[Xe]5d^1 \rightarrow [Xe]4f^1$ interconfigurational electron transitions. Inserting Na^+ and V^{5+} ions into the YAG:Ce^{3+} matrix, the Ce^{3+} emission intensity decreased, due to the occurring defects. The emission spectra of Tb^{3+} doped garnets were dominated by the lines in the wavelength range of 350–700 nm with a maximum at 542 nm ($^5D_4 \rightarrow {}^7F_5$ transition). Inserting Na^+ ions into the YAG:Tb^{3+} matrix did not change the emission intensity of Tb^{3+}, while after inserting V^{5+} ions, the Tb^{3+} emission decreased almost 10 times. The emission spectra of Eu^{3+} doped garnets showed the most intense Eu^{3+} emission line at 709 nm, which originates from the $^5D_0 \rightarrow {}^7F_4$ transition. Doping YAG:Eu^{3+} matrix with Na^+ did not have any effect on the intensity of the Eu^{3+} emission, while doping with V^{5+} ions, the Eu^{3+} emission reduced almost 9 times. It is important to note that emission of Ce^{3+}-doped phosphors occurs in the green-yellow spectral range, Tb^{3+}-doped – in the yellowish-green spectral range, and Eu^{3+}-doped – in the reddish-orange spectral range. To conclude, the investigated new garnet-type luminophores are interesting compounds with novel chemical compositions and are potential candidates for various optical applications.

CRediT authorship contribution statement

Diana Vistorskaja: Investigation, Data curation. **Arturas Katelnikovas:** Validation, Formal analysis, Data curation. **Carlos Martin Signes:** Investigation, Data curation. **Vytautas Klimavicius:** Writing – original draft, Visualization. **Anna Lukowiak:** Formal analysis, Data curation, Conceptualization. **Wieslaw Strenk:** Project administration, Funding acquisition. **Aivaras Kareiva:** Writing – review & editing, Supervision, Methodology.

Declaration of competing interest

The article is original.

The article has been written by the stated authors who are ALL aware of its content and approve its submission.

The article has not been published previously.

The article is not under consideration for publication elsewhere.

No conflict of interest exists, or if such conflict exists, the exact nature must be declared.

If accepted, the article will not be published elsewhere in the same form, in any language, without the written consent of the publisher.

Data availability

No data was used for the research described in the article.

Acknowledgements

Vilnius University is highly acknowledged for support from the Science Promotion Foundation (MSF-JM-5/2022). The center SPECTROVERSUM (https://www.spectroversum.ff.vu.lt) is acknowledged for use of solid-state NMR spectroscopic equipment.

Appendix A. Supplementary data

Supplementary data to this article can be found online at https://doi.org/10.1016/j.omx.2024.100300.

References

[1] G.B. Nair, H.C. Swart, S.J. Dhoble, A review on the advancements in phosphor-converted light emitting diodes (pc-LEDs): phosphor synthesis, device fabrication and characterization, Prog. Mater. Sci. 100622 (2019) 1–11, https://doi.org/10.1016/j.pmatsci.2019.100622.

[2] Z. Xia, Q. Liu, Progress in discovery and structural design of color conversion phosphors for LEDs, Prog. Mater. Sci. 84 (2016) 59–117, https://doi.org/10.1016/j.pmatsci.2016.09.007.

[3] Q. Yao, P. Hu, P. Sun, M. Liu, R. Dong, K. Chao, Y. Liu, J. Jiang, H. Jiang, YAG:Ce^{3+} transparent ceramic phosphors brighten the next-generation laser-driven lighting, Adv. Mater. 32 (19) (2020) 1907888, https://doi.org/10.1002/adma.201907888.

[4] G. Li, Q. Cao, Z. Li, Y. Huang, Y. Wei, J. Shi, Photoluminescence properties of YAG:Tb nano-powders under vacuum ultraviolet excitation, J. Alloys Compd. 485 (1–2) (2019) 561–564, https://doi.org/10.1016/j.jallcom.2009.06.026.

[5] P.F.S. Pereira, M.G. Matos, L.R. Ávila, E.C.O. Nassor, A. Cestari, K.J. Ciuffi, P. S. Calefi, E.J. Nassar, Red, green and blue (RGB) emission doped $Y_3Al_5O_{12}$ (YAG) phosphors prepared by non-hydrolytic sol–gel route, J. Lumin. 130 (3) (2010) 488–493, https://doi.org/10.1016/j.jlumin.2009.10.019.

[6] J.C.A. Santos, E.P. Silva, D.V. Sampaio, Y.G.S. Alves, M.V.S. Rezende, C. Kucera, J. Ballato, R.S. Silva, Structural, microstructural, and luminescent properties of laser-sintered Eu-doped YAG ceramics, Opt. Mater. 89 (2019) 334–339, https://doi.org/10.1016/j.optmat.2019.01.038.

[7] Georges Boulon, Fifty years of advances in solid-state laser materials, Opt. Mater. 34 (2012) 499–512, https://doi.org/10.1016/j.optmat.2011.04.018.

[8] H. Yang, Y.S. Kim, Energy transfer-based spectral properties of Tb-, Pr-, or Sm-codoped YAG:Ce nanocrystalline phosphors, J. Lumin. 128 (10) (2008) 1570–1576, https://doi.org/10.1016/j.jlumin.2008.03.003.

[9] D. Vistorskaja, A. Laurikenas, A. Montejo de Luna, A. Zarkov, S. Pazylbek, A. Kareiva, Sol-gel synthesis and characterization of novel $Y_{3-x}M_xAl_{5-y}V_yO_{12}$ (M—Na, K) garnet-type compounds, Inorganics 11 (58) (2023), https://doi.org/10.3390/inorganics11020058.

[10] Y. Zhydachevskii, I.I. Syvorotka, L. Vasylechko, D. Sugak, I.D. Borshchyshyn, A. P. Luchechko, Y.I. Vakhula, S.B. Ubizskii, M.M. Vakiv, A. Suchocki, Crystal structure and luminescent properties of nanocrystalline YAG and YAG:Nd synthesized by sol–gel method, Opt. Mater. 34 (12) (2012) 1984–1989, https://doi.org/10.1016/j.optmat.2011.12.023.

[11] S.A. Hassanzadeh-Tabrizi, Low temperature synthesis and luminescence properties of YAG: Eu nanopowders prepared by modified sol-gel method, T. Nonferr. Metal. Soc. 21 (11) (2011) 2443–2447, https://doi.org/10.1016/S1003-6326(11)61034-0.

[12] T. Hua, Q. Zeng, J. Qi, G. Cheng, X. Chen, Z. Huang, Q. Zhang, X. Huang, X. Guo, N. Wei, T. Lu, Effect of calcium oxide doping on the microstructure and optical properties of YAG transparent ceramics, Mater. Res. Express 6 (2018), https://doi.org/10.1088/2053-1591/aaf487.

[13] X. Zhou, K. Zhou, Y. Li, Z. Wang, Q. Feng, Luminescent properties and energy transfer of $Y_3Al_5O_{12}$:Ce^{3+}, Ln^{3+} (Ln = Tb, Pr) prepared by polymer-assisted sol–gel method, J. Lumin. 132 (11) (2012) 3004–3009, https://doi.org/10.1016/j.jlumin.2012.06.005.

[14] J.H. In, H.C. Lee, M.J. Yoon, K.K. Lee, J.W. Lee, C.H. Lee, Synthesis of nano-sized YAG:Eu^{3+} phosphor in continuous supercritical water system, J. Supercrit. Fluids 40 (3) (2007) 389–396, https://doi.org/10.1016/j.supflu.2006.08.006.

[15] D.A. Hora, A.B. Andrade, N.S. Ferreira, V.C. Teixeira, M.V. dos S. Rezende, X-ray excited optical luminescence of Eu-doped YAG nanophosphors produced via glucose sol–gel route, Ceram. Int. 42 (8) (2016) 10516–10519, https://doi.org/10.1016/j.ceramint.2016.03.142.

[16] M. Borlaf, M. Frankowska, W.W. Kubiak, T. Graule, Strong photoluminescence emission at low dopant amount in YAG:Ce and YAG:Eu phosphors, Mater. Res. Bull. 100 (2018) 413–419, https://doi.org/10.1016/j.materresbull.2018.01.005.

[17] G. Xia, S. Zhou, J. Zhang, S. Wang, Y. Liu, J. Xu, Sol–gel combustion synthesis and luminescent properties of nanocrystalline YAG:Eu^{3+} phosphors, J. Cryst. Growth 283 (1–2) (2005) 257–262, https://doi.org/10.1016/j.jcrysgro.2005.05.060.

[18] G. Dantelle, M. Salaün, R. Bruyère, S. Kodjikian, A. Ibanez, Luminescent coatings prepared from optimized YAG:Ce nanoparticles, Thin Solid Films 643 (2017) 36–42, https://doi.org/10.1016/j.tsf.2017.05.001.

[19] S. Mukherjee, V. Sudarsan, R.K. Vatsa, A.K. Tyagi, Luminescence studies on lanthanide ions (Eu^{3+}, Dy^{3+} and Tb^{3+}) doped YAG:Ce nano-phosphors, J. Lumin. 129 (1) (2009) 69–72, https://doi.org/10.1016/j.jlumin.2008.08.003.

[20] Y. Zhou, J. Lin, M. Yu, S. Wang, H. Zhang, Synthesis-dependent luminescence properties of $Y_3Al_5O_{12}$:Re^{3+} (Re=Ce, Sm, Tb) phosphors, Mater. Lett. 56 (2002) 628–636, https://doi.org/10.1016/S0167-577X(02)00567-0.

[21] J. Zhang, J. Ning, X. Liu, Y. Pan, L. Huang, Synthesis of ultrafine YAG:Tb phosphor by nitrate–citrate sol–gel combustion process, Mater. Res. Bull. 38 (7) (2003) 1249–1256, https://doi.org/10.1016/S0025-5408(03)00119-3.

[22] M. Skruodiene, R. Juodvalkyte, M. Kemere, R. Ramanauskas, A. Sarakovskis, R. Skaudzius, Enhanced optical properties of yttrium aluminum garnet with the yttrium vanadate impurity phase, Heliyon 8 (11) (2022) e11386, https://doi.org/10.1016/j.heliyon.2022.e11386.

[23] G. Inkrataite, A. Pakalniskis, S. Pazylbek, D. Vistorskaja, R. Skaudzius, A. Kareiva, Sol-gel synthesis and characterization of praseodymium-doped and calcium-, titanium-substituted yttrium aluminium garnets Pr:$Y_{3-x}Ca_xAl_{5-y}Ti_yO_{12}$, Mater. Sci. Eng., B 285 (2022), https://doi.org/10.1016/j.mseb.2022.115963.

[24] Y. Ding, X. Zhang, H. Zhua, J. Zhu, A lanthanide-doping route to aspect-ratio-controlled KSc_2F_7 nanocrystals for upconversion, downconversion and magnetism, J. Mater. Chem. C 2 (2014) 946–951, https://doi.org/10.1039/C3TC31608D.

[25] M. Zhou, H. Chen, X. Zhang, B. Tang, Phase composition, microstructure, and microwave dielectric properties of non-stoichiometric yttrium aluminum garnet ceramics, J. Eur. Ceram. Soc. 42 (2) (2022) 472–477, https://doi.org/10.1016/j.jeurceramsoc.2021.10.040.
[26] D. Karoblis, K. Mazeika, R. Raudonis, A. Zarkov, A. Kareiva, Sol-gel synthesis and characterization of yttrium-doped MgFe2O4 spinel, Materials 15 (21) (2022) 7547, https://doi.org/10.3390/ma15217547.
[27] A. Boukerika, L. Guerbous, M. Belamri, Effect of different annealing atmospheres on the structural and luminescence properties of Ce^{3+}-doped YAG phosphors synthesized by sol–gel method, Optik 127 (13) (2016) 5235–5239, https://doi.org/10.1016/j.ijleo.2016.03.037.
[28] V.V. Bakhmetyev, T.S. Minakova, S.V. Mjakin, L.A. Lebedev, A.B. Vlasenko, A. A. Nikandrova, A. Ringuede, Synthesis and surface characterization of nanosized Y_2O_3:Eu and YAG:Eu luminescent phosphors which are useful in photodynamic therapy of cancer, Eur. J. Nanomed. 8 (4) (2016) 173–184, https://doi.org/10.1515/ejnm-2016-0020.
[29] A. Potdevin, G. Chadeyron, D. Boyer, R. Mahiou, Sol-gel elaboration and characterization of YAG:Tb^{3+} powdered phosphors, J. Mater. Sci. 41 (8) (2006) 2201–2209, https://doi.org/10.1007/s10853-006-7182-7.
[30] P. Florian, M. Gervais, A. Douy, D. Massiot, J.P. Coutures, A multi-nuclear multiple-field nuclear magnetic resonance study of the Y_2O_3−Al_2O_3 phase diagram, J. Phys. Chem. B 105 (2) (2001) 379–391, https://doi.org/10.1021/jp0008851.
[31] L. Pavasaryte, A. Katelnikovas, V. Klimavicius, V. Balevicius, A. Krajnc, G. Mali, J. Plavec, A. Kareiva, Eu^{3+}-Doped $Y_3Nd_xAl_3O_{12}$ garnet: synthesis and structural investigation, Phys. Chem. Chem. Phys. 19 (5) (2017) 3729–3737, https://doi.org/10.1039/C6CP07723D.
[32] L. Pavasaryte, A. Katelnikovas, V. Klimavicius, V. Balevicius, A. Momot, M. Van Bael, A. Hardy, A. Kareiva, Eu^{3+}-Doped $Y_3Sm_xAl_3O_{12}$ garnet: synthesis and structural investigation, New J. Chem. 42 (2018) 2278–2287, 10.1039.C7NJ03468G.
[33] S. Bradley, J. Hanna, Aluminium-27 MAS NMR investigations of sodium aluminates formed from high pH solutions: evidence of a complex polymer containing both four- and six-coordinate aluminium, J. Chem. Soc. Chem. Commun. 16 (1993) 1249–1251, https://doi.org/10.1039/C39930001249.
[34] T. Graham, M. Dembowski, E. Martinez-Baez, X. Zhang, N. Jaegers, J. Hu, M. Gruszkiewicz, H. Wang, A. Stack, M. Bowden, C. Delegard, G. Schenter, A. Clark, S. Clark, A. Felmy, K. Rosso, C. Pearce, In situ ^{27}Al NMR spectroscopy of aluminate in sodium hydroxide solutions above and below saturation with respect to gibbsite, Inorg. Chem. 57 (19) (2018) 11864–11873, https://doi.org/10.1021/acs.inorgchem.8b00617.
[35] R. Amantea, P. Ghigna, P. Mustarelli, V. Tartara, Synthesis, ^{89}Y and ^{51}V-NMR of Er-doped zircon-type YVO_4 and $LUVO_4$, J. Solid State Chem. 178 (5) (2005) 1692–1696, https://doi.org/10.1016/j.jssc.2005.03.014.
[36] S.K. Lee, J.F. Stebbins, The distribution of sodium ions in aluminosilicate glasses: a high-field Na-23 MAS and 3Q MAS NMR study, Geochem. Cosmochim. Acta 67 (9) (2003) 1699–1709, https://doi.org/10.1016/S0016-7037(03)00026-7.
[37] R. McCarty, J. Stebbins, Investigating lanthanide dopant distributions in Yttrium Aluminum Garnet (YAG) using solid state paramagnetic NMR, Solid State Nucl. Mag. 79 (2016) 11–22, https://doi.org/10.1016/j.ssnmr.2016.10.001.
[38] T. Harazono, E. Yokota, H. Uchida, T. Watanabe, ^{89}Y-static and-MAS NMR, and ^{27}Al-MAS NMR in green phosphor, Tb-doped $Y_3Al_5O_{12}$ and luminous characteristics, Bull. Chem. Soc. Jpn. 71 (12) (1998) 2797–2805, https://doi.org/10.1246/bcsj.71.2797.
[39] R. Skaudzius, J. Pinkas, R. Raudonis, A. Selskis, R. Juskenas, A. Kareiva, On the limitary radius of garnet structure compounds $Y_3Al_{5x}M_xO_{12}$ (M = Cr, Co, Mn, Ni, Cu) and $Y_3Fe_{5x}Co_xO_{12}$ ($0 \leq x \leq 2.75$) synthesized by solegel method, Mater. Chem. Phys. 135 (2012) 479–485, https://doi.org/10.1016/j.matchemphys.2012.05.011.
[40] M. Singlard, F. Rémondière, S. Oriol, G. Fiore, B. Vieille, M. Vardelle, S. Rossignol, Sol-gel synthesis of yttrium aluminum garnet (YAG): effects of the precursor nature and concentration on the crystallization, J. Sol-gel Sci. Techn. 87 (2018) 496, https://doi.org/10.1007/s10971-018-4722-y.
[41] A. Katelnikovas, Synthesis and Characterization of Luminescent Materials for Solid State Light Sources, Doctoral dissertation, Vilnius University, 2012.
[42] R. Skaudžius, Synthesis and Investigation of Co-doped Yttrium Aluminium and Yttrium Gallium Garnets, Doctoral dissertation, Vilnius University, 2014.
[43] S. Zhou, Z. Fu, J. Zhang, S. Zhang, Spectral properties of rare-earth ions in nanocrystalline YAG:Re (Re=Ce^{3+}, Pr^{3+}, Tb^{3+}), J. Lumin. 118 (2) (2006) 179–185, https://doi.org/10.1016/j.jlumin.2005.08.011.
[44] G. Blasse, B.C. Grabmaier, Luminescent Materials, Spinger-Verlag, Berlin, 1994.
[45] M. Skruodiene, A. Katelnikovas, L. Vasylechko, R. Skaudzius, Tb^{3+} to Cr^{3+} energy transfer in a Co-doped $Y_3Al_5O_{12}$ host, J. Lumin. 208 (2019) 327–333, https://doi.org/10.1016/j.jlumin.2018.12.048.
[46] Y.K. Jung, H.W. Lee, Enhanced luminescent properties of $Y_3Al_5O_{12}$:Tb^{3+},Ce^{3+} phosphor prepared by spray pyrolysis, J. Lumin. 126 (2) (2007) 469–474, https://doi.org/10.1016/j.jlumin.2006.09.009.
[47] K. Binnemans, Interpretation of europium(III) spectra, Coord. Chem. Rev. 295 (2015) 1–45, https://doi.org/10.1016/j.ccr.2015.02.015.